Temporally correlated active forces drive chromosome structure and dynamics

Sumitabha Brahmachari,[1,*] Tomer Markovich,[1,2,3] Fred C. MacKintosh,[1,4,5] and José N. Onuchic[1,6,5]

[1] *Center for Theoretical Biological Physics, Rice University, Houston, TX 77005, USA*
[2] *School of Mechanical Engineering, Tel Aviv University, Tel Aviv 69978, Israel*
[3] *Chemistry of Living Systems, Tel Aviv University, Tel Aviv 69978, Israel*
[4] *Department of Chemical and Biomolecular Engineering, Rice University, Houston, TX 77005, USA*
[5] *Department of Physics and Department of Chemistry, Rice University, Houston, TX 77005, USA*
[6] *Department of Biosciences, Rice University, Houston, TX 77005, USA*

Understanding the mechanisms governing the structure and dynamics of flexible polymers like chromosomes, especially, the signatures of motor-driven active processes is of great interest in genome biology. We study chromosomes as a coarse-grained polymer model where microscopic motor activity is captured via an additive temporally persistent noise. The active steady state is characterized by two parameters: active force, controlling the persistent-noise amplitude, and correlation time, the decay time of active noise. We find that activity drives dynamic compaction, leading to a globally collapsed entangled globule for long correlation times. Diminished topological constraints destabilize the entangled globule, and the polymer segments trapped in the globule move toward the periphery, resulting in an enriched density near the periphery. We also show that heterogeneous activity may lead to the segregation of the highly dynamic species from the less dynamic one. Our model suggests correlated motor forces as a factor (re)organizing chromosome compartments and driving transcriptionally active regions towards the chromosome periphery. This contrasts the passive adhesive or repulsive forces shaping chromosome structures. Importantly, structural ensembles are not sufficient to distinguish between the active or passive mechanisms, but the dynamics may hold key distinguishing signatures. The motor-driven polymer shows distinctive dynamic features like enhanced apparent diffusivity and exploration of all the dynamic regimes (sub-diffusion, effective diffusion, and super-diffusion) at various lag times.

INTRODUCTION

Active processes, driven by molecular motors that consume energy (ATP) and exert persistent forces on biopolymers, are ubiquitous and crucial for sustaining cellular life. While motor-driven phenomena like network contractility [1–3] and motility [4–7] are well studied for stiff cytoskeletal polymer networks, the mechanical consequences of activity remain poorly explored for flexible polymers in the context of genome organization.

Folded chromosomes occupy mutually exclusive territories [8–10], where specific pairs of segments are more likely to be three-dimensional neighbors than others [11–15]. Chromatin bearing distinct epigenetic markers of transcriptional activity (euchromatin and heterochromatin) preferentially interact among themselves, forming A and B compartments [11, 16]. A characteristic structural feature is the organization of B compartments inside, and A compartments towards the periphery of chromosome territories [9, 17, 18]. Data-driven effective-equilibrium polymer models, via optimizing the inter-monomer-interaction energies, generate ensembles of folded structures consistent with experimental observations like contact frequencies [18–27]. These models, however, lack a direct connection to physical driving and are insufficient to explore the motor-driven aspects of chromosome structure and dynamics.

Chromosome dynamics is typically sub-diffusive at short time scales (seconds), as expected for a polymer [28–31]. However, there is significant heterogeneity in loci dynamics, reflected in altered mobility subgroups within the distribution of apparent diffusion constants [32–36]. In the effective-equilibrium approach, the altered mobility has been reasoned to arise from local confinement and/or the local compaction state [33, 37]. These structure-centric approaches are limited to only reducing the apparent diffusivity as compared to a free Brownian particle. The possibility of motor-activity-driven enhancement of dynamics is beyond such approaches. Noteworthy, some chromatin loci have been observed to move super-diffusively at intermediate time scales [35, 38, 39], which is at odds with any effective-equilibrium or passive approach.

We propose an active chromosome model where motor-generated forces within a coarse-grained locus contribute to its mobility. Within the active paradigm, coarse-grained motor activity contributes an additive noise that is temporally correlated (see Eq. (1) below). Active dynamics span sub-diffusion, effective diffusion, and super-diffusion. The apparent diffusion of a locus at long lag times is enhanced proportionally to the activity at the locus. Notably, activity not only introduces dynamical heterogeneity, but also affects the chromosome structure. Processes like transcription [40, 41], chromatin remodeling [42, 43], and loop extrusion [44, 45], that rely on ATP-consuming motors and exert forces on chromatin, are the hypothesized sources of activity.

To highlight the main features of motor activity in the chromosome we consider a minimal model: a confined active polymer with soft self-avoidance. This

model exhibits contrasting structural features like polymer swelling, collapse into an entangled globule, and enrichment of monomer density near confinement boundaries. These biologically relevant structural characteristics are dynamics-driven emergent properties of the active steady state. Whereas, in effective-equilibrium models, these structures are a result of optimizing passive parameters like inter-monomer interactions and stiffness of bonds [18, 19, 46, 47]. Interestingly, the steady state structure is not enough to distinguish active and passive models. The active steady-state polymer conformations may look identical to the passive ones of a completely unrelated system. Such as the collapsed globule of a purely self-avoiding active polymer may structurally disguise as a passive polymer with inter-monomer attractions. This highlights a potential ambiguity in deciphering the underlying mechanism from structural ensembles alone. However, signatures of enhanced dynamics like super-diffusion or high apparent diffusivity of the polymer unambiguously point towards the active model.

The layout of the article is as follows. We first describe the active polymer model and introduce the parameters: active force and correlation time that characterize activity (Fig. 1). Next, we investigate the steady state of a confined, active homopolymer (Fig. 2). Then, to understand the consequences of heterogeneous activity, we simulate an active-passive block copolymer, uncovering features like phase segregation of active and passive monomers (Fig. 3). Building upon the intuition from the homopolymer and the block copolymer models, we discuss the model's relevance to chromosomes. By adding active loci to a passive chromosome model (MiChroM [19, 48]), we explore how the enhanced dynamics of an active locus perturbs the local structure (Fig. 4). Finally, we conclude with an overview and discussion.

RESULTS

Active polymer model

The active polymer model hypothesizes molecular motors as force dipoles [49–55]. The length of each dipole is much smaller than the coarse-grained monomer diameter, hence there are multiple microscopic motors pushing and pulling inside a monomer (Fig. 1). The net active force on a monomer due to the microscopic motors vanishes when averaged over ensembles or long times. However, the motor binding kinetics makes the active force correlated over short time scales, set by the motor-residence time. This results in noise-like active kicks that are temporally correlated. The temporal decay of correlations is determined by the distribution of residence times of the motors. If motor (un)binding events are independent, the residence times follow a Poisson distribution giving an exponentially correlated noise. Following previous approaches [51, 53–56], we assume that the active force correlation decays exponentially, characterized by a single time scale τ, the correlation time.

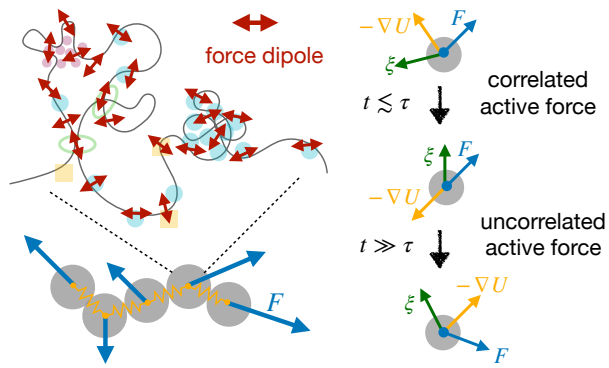

FIG. 1. **Schematic active polymer model.** Microscopic motors exerting forces on the polymer are depicted as small red force dipoles. Each coarse-grained monomer containing the force dipoles experiences an active noise with amplitude F. At each time step, every monomer experiences three kinds of forces (Eq. (1)): temporally uncorrelated thermal noise ξ, passive forces derived from the polymer potential $-\nabla U$, and the active force F. The active kicks are correlated over a time scale τ, the correlation time. When averaged over long lag times ($t \gg \tau$), the correlation of the active kicks vanishes (Eq. (2))

The overdamped equation of motion of the n-th active monomer in a thermal bath at temperature T reads as follows.

$$\gamma \frac{dr_n}{dt} = -\nabla_n U + \xi_n(t) + f_n(t) \tag{1}$$

Here, γ is the drag coefficient, and $-\nabla_n U$ represents the passive forces derived from the polymer potential, like the harmonic bonds between nearest neighbors. Random forces from thermal fluctuations, represented by ξ_n, are uncorrelated: $\langle \xi_n(t)\xi_m(t')\rangle = 2\gamma k_B T \delta(t-t')\delta_{mn}$, where k_B is the Boltzmann constant. The active noise f_n, unlike thermal fluctuations, is correlated.

$$\langle f_n(t) f_m(t')\rangle = F^2 \exp(-|t-t'|/\tau)\delta_{mn} \tag{2}$$

The amplitude of active noise F, a free parameter in the model, is expected to scale with the number of motors within the monomer. Note, we assume that the active forces of the neighboring coarse-grained monomers are uncorrelated. We ignore explicit correlations of the active force along the coarse-grained polymer contour, which may be of biological interest [57], and is left for future work. Including the effect of torque-inducing motors is yet another biologically relevant future possibility [58].

The technique of representing activity as a correlated noise has been discussed both in the context of motor activity in the cytoskeleton [49, 51, 56, 59, 60], as well as for active colloidal solutions, where the term Active

Ornstein-Uhlenbeck Particles (AOUPs) is used [61, 62]. The steady state of AOUPs shows remarkable features such as inhomogeneous density profiles in confinement and Motility-Induced Phase Separation (MIPS): self-avoiding AOUPs segregate into a dense phase, mimicking effective attractive interactions [63]. The AOUP model has also been adopted to study Active Rouse polymers [54, 55, 64]. These polymer models focus on dynamics, while structural features, such as the analog of MIPS, remain largely unexplored.

Mean persistent path and the active steady state

The steady state of the active polymer is governed by a competition between the active (F, τ) and passive (T) parameters. A metric of activity is the emergent length: $\lambda_a \equiv F\tau/\gamma$, which we call the *mean persistent path* of an active monomer. This is the average distance an active monomer moves persistently before changing direction. In presence of thermal fluctuations of strength T, the active features dominate only when the active temperature-like quantity $\theta_a = F\lambda_a$ is dominant: $\theta_a > T$. Another regime where thermal effects dominate is when the active noise amplitude is weaker than the thermal noise amplitude: $F < k_BT/\sigma$, where σ is the monomer diameter that is used as a unit of distance. Hence, we refer to the parameter regime with $\theta_a > T$ and $F > k_BT/\sigma$ as the active steady state and $\theta_a < T$ or $F < k_BT/\sigma$ as the thermal-dominated passive-like steady state (Figs. 2A, 3B). The simulation unit of energy is ϵ, such that forces are measured in ϵ/σ. The unit of time is $\tau_\sim = \eta\sigma^3/\epsilon$, where η is the viscosity.

Self-avoiding active homopolymer in confinement

The physics underlying the active model (Eq. (1)) has been explored in the context of Rouse chains [54, 55, 64], which is in agreement with our simulations (Supplementary Material, Fig. S1). Here, we study the behavior of an active homopolymer with biologically relevant constraints: self-avoidance and confinement. Fig. 2 shows the results for a self-avoiding polymer with $N = 2000$ monomers that is confined within a sphere of radius $R_c = 16\sigma$, such that the volume fraction: $\phi \equiv N\sigma^3/(2R_c)^3 \approx 6\%$, is in the physiological regime for confined chromatin [65]. For details of the potentials, see Methods.

Activity drives dynamic compaction in self-avoiding polymers

A prominent signature of the active steady state is the compaction of a self-avoiding polymer into a denser globule with a lower radius of gyration than the passive case (Fig. 2A). The compact state emerges when the mean persistent path λ_a exceeds the average spacing between monomers, given by the concentration-dependent distance: $\lambda_{\text{coll}} \approx \sigma/\phi^{1/3}$. In this regime ($\lambda_a > \lambda_{\text{coll}}$), active monomers even after colliding with each other maintain their active noise direction, resulting in them getting trapped in a dynamically driven dense state. The compact state is characterized by dense clusters that coexist with less dense regions, where the correlation time dictates the stability of the compact clusters.

Activity correlated over long times establishes a collapsed, entangled globule

Activity with a long correlation time traps the polymer into a globally collapsed globule (Fig. 2A). The collapsed globule is stabilized by topological entanglements, making the globule a long-lived state. The polymer segments on the periphery of the globule may reorient their average active noise direction to escape the collapsed state. This leads to some segments coexisting in a less dense state with the entangled collapsed globule (Fig. 2D). Such segments, however, after momentarily exploring the less dense space outside the globule, reencounter the dense state, thus keeping the globule from dissociating. The compact structures driven by activity are liquid-like, however, the entangled globule exhibits an enhanced solid-like packing and mechanical integrity (Fig. 2C).

The collapsed globule is reminiscent of the segregated state in active colloids exhibiting MIPS [61, 63]. The collapsed state occurs at a lower density in active polymers ($\phi \sim 0.05$) compared to AOUPs ($\phi \sim 0.5$) [61, 66]. This stems from polymer entanglements stabilizing the dense phase.

Large noise amplitudes destabilize the collapsed globule via stretching bonds and reducing entanglements.

The collapsed, entangled globule gradually disappears as the active noise amplitude F is increased (Fig. 2A). Increasing the active force F increases the fraction of the polymer that coexists in the less dense space outside the globule, eventually leading to the complete destabilization of the dense state. This destabilization is due to the stretching of the bonds of the polymer by strong active kicks, which diminishes the topological constraints. Two non-neighboring segments with stretched bonds are more likely to pass through each other than get trapped in a dense state. We find that $\approx 25\%$ increase in the average bond length is enough to destabilize the collapsed state (Fig. 2A, E).

In accordance with our rationale, increasing the bond stiffness, which decreases the bond length and reinforces

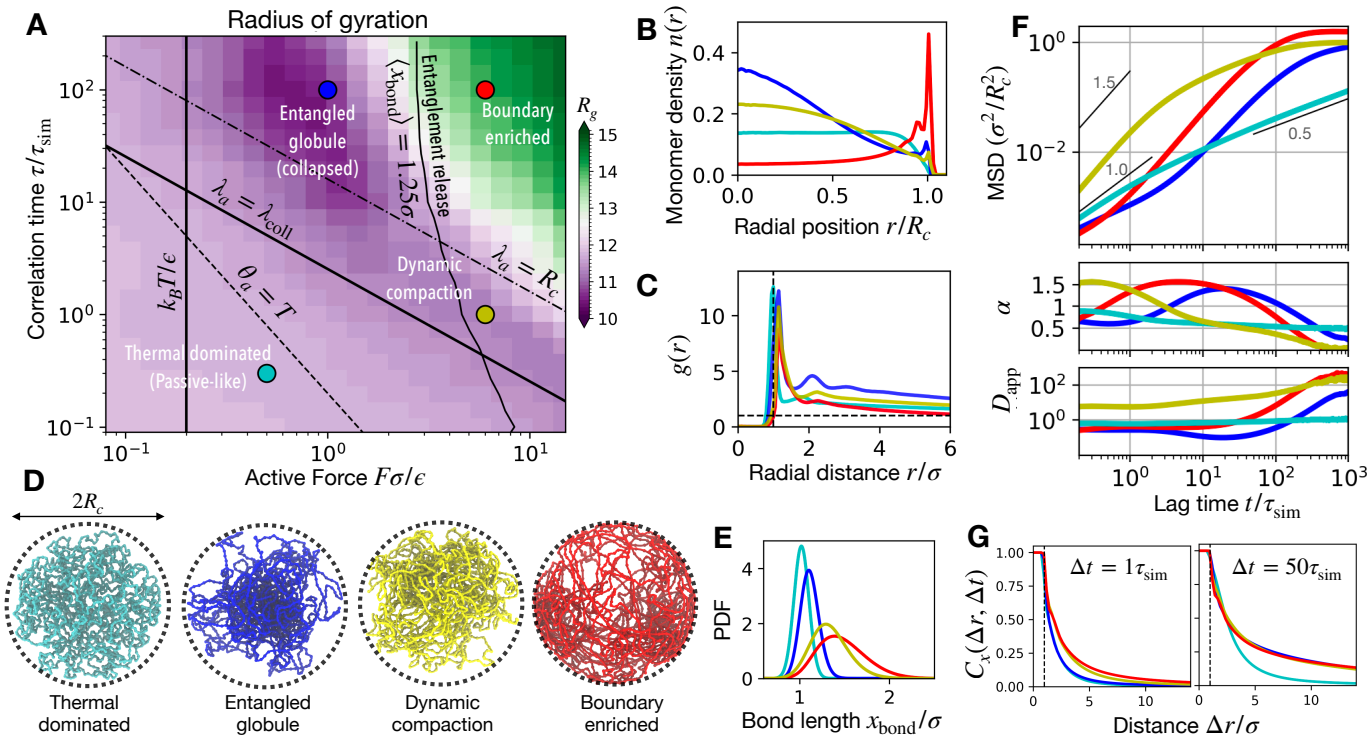

FIG. 2. **Self-avoiding active polymer in spherical confinement.** (A) Active regime diagram spanned by the active force F (ϵ/σ units) and the correlation time τ ($\tau_{\rm sim}$ units). The colors depict radius of gyration (R_g) of the polymer (σ units). The active steady state ($F > k_BT/\sigma$ and $\theta_a > T$) shows compaction when the mean persistent path $\lambda_a \equiv F\tau/\gamma$, is longer than the mean collision distance between the monomers $\lambda_{\rm coll} = \sigma/\phi^{1/3}$, where ϕ is the confinement volume fraction. This compaction is characterized by short-lived (dynamic) locally collapsed clusters. Long correlation times lead to a globally collapsed, entangled globule state. When λ_a is greater than the confinement dimension R_c, the monomers have a tendency to get trapped at the boundary wall. However, release of entanglements is necessary to destabilize the competing entangled-globule state in order to enrich the boundaries. Hence only when the bonds are stretched by the active force (mean bond distance $\langle x_{\rm bond}\rangle > 1.25\sigma$), leading to entanglement release, does the boundary-enriched state appear. Representative parameter sets for the four regimes are shown in colored circles for which various observables are plotted: thermal dominated ($F = 0.5$, $\tau = 0.3$, cyan), entangled globule ($F = 1$, $\tau = 100$, blue), dynamic compaction ($F = 6$, $\tau = 1$, yellow), and boundary enriched ($F = 6$, $\tau = 100$, red). We used $k_BT = 0.2\epsilon$ for all simulations. (B) Radial profile of the monomer number density $n(r)$. (C) Radial distribution function $g(r)$ shows a peak at 1σ corresponding to self-avoidance. Only the entangled globule state shows prominent successive peaks reflecting the collapsed state and an increased solid-like behavior. (D) Representative simulation snapshots where the dotted line represents the spherical confinement with radius R_c. Note that the collapsed structures may appear as a passive polymer with self-adhesion, while the boundary-enriched state might resemble a passive polymer with boundary adhesion. This refers to the ambiguity in deciphering the underlying mechanism from structural ensembles alone. (E) Bond length distribution showing the increase in the mean bond length $\langle x_{\rm bond}\rangle$ for higher active force F. (F) Mean-squared displacement (MSD), normalized by the confinement dimensions, versus lag time t ($\tau_{\rm sim}$ units), where the scaling exponents 0.5, 1.0, and 1.5 are drawn for comparison. The dynamic exponent α, and the apparent diffusivity $D_{\rm app}$, are plotted in the subpanels below. Active steady states span sub-diffusion, effective diffusion, and super-diffusion. The exponent α goes to zero at long lag times due to the confinement-induced saturation of MSD. (G) Correlation of monomer displacements measured over Δt, plotted as a function of the distance between the monomers Δr. Active steady states show enhanced correlated motion.

the entanglement constraints, stabilizes the collapsed state for higher noise amplitudes (Fig. S4). The stability of the entangled globule state for low active noise amplitudes is governed by the thermal temperature. When $F < k_BT/\sigma$, uncorrelated thermal noise dominates the correlated active noise, leading to destabilization of the collapsed, entangled state (Figs. 2A, S5).

Competition between mean persistent path and confinement dimension leads to boundary enriched polymer.

A boundary-enriched state emerges for high active force and high correlation times, where the monomer density peaks at the boundary, is depleted at the center, and the polymer is expanded such that the radius of gyration assumes the size of the box (Fig. 2A, B). When the mean persistent path is longer than the confinement dimension, i.e., $\lambda_a > R_c$, the active monomers collapse on

the boundary wall. The active monomers with long correlation times keep pushing against the wall, while upon reorientation of their active force direction, they move in a correlated fashion until encountering the other side of the boundary. However, this state only appears when the entanglement-driven constraints are sufficiently weaker so that the polymer does not get trapped in the entangled globule state. Hence, the two criteria for the appearance of this state are the high force, necessary for the release of entanglements, and a high enough mean persistent path, necessary for getting trapped at the boundary (Fig. 2A).

Boundary enrichment comes about from a competition between monomer activity and confinement, hence, self-avoidance and polymer connectivity are not necessary for establishing this state. As a result, active Rouse chains and active gas or colloidal particles particles (AOUPs) both exhibit emergence of boundary enrichment with appropriate mean persistent path (Figs. S2 and S3).

Structural ensembles are insufficient to distinguish between effective-equilibrium and actively driven phenomena

The conformations of the active steady state may appear to belong to a completely unrelated passive system. For example, the collapsed state might look like a polymer with self-adhesive interactions (Fig. 2D). Or, the boundary-enriched structures may appear as though the monomers have attractive interactions with the confinement wall (Fig. 2D). This clearly suggests that structural ensembles are not enough to distinguish between the underlying active and passive mechanisms. However, the dynamics may hold key distinguishing features.

Regimes of polymer dynamics

The dynamics in viscoelastic media is often characterized by anomalous diffusion, with the mean-squared displacement (MSD) given by $\langle (r_n(s+t) - r_n(s))^2 \rangle = Dt^\alpha$, where the dynamical exponent of the lag time t classifies distinct dynamic regimes: diffusion for $\alpha = 1$, sub-diffusion for $\alpha < 1$ and super-diffusion for $\alpha > 1$. The coefficient D is an apparent diffusivity parameter. A free passive particle executes diffusion, where D is the diffusion constant proportional to the thermal temperature: $D_{\text{free}} = k_B T/\gamma$.

Polymer relaxation spans multiple time scales that arise because fluctuations with longer wavelengths decay slower. The shortest wavelength fluctuations, corresponding to bond fluctuations, relax at short time scales $\tau_{\text{bond}} \sim \gamma/k$, where k is the bond stiffness. On the other end of the spectrum, $\tau_{\text{Rse}} \approx N^2\gamma/(k\pi^2)$ corresponds to the relaxation time of the longest wavelength [67] (see Supplementary Materials; for Figs. 2 and 3, $\tau_{\text{bond}} \approx 0.1\tau_{\text{sim}}$ and $\tau_{\text{Rse}} \approx 10^4\tau_{\text{sim}}$, where τ_{sim} is the unit of simulation time). The third important time scale is the active correlation time τ. An interplay of these time scales determines the dynamic signatures.

For lag times shorter than the bond relaxation time ($t \ll \tau_{\text{bond}} < \tau$), passive polymer dynamics resembles free-particle diffusion (Fig. 2F). For lag times larger than the bond relaxation but smaller than the longest polymer relaxation time ($\tau_{\text{bond}} < t < \tau_{\text{Rse}}$), passive dynamics exhibits sub-diffusion ($\alpha < 1$) (Fig. 2F) [67]. This originates from each monomer having to drag a portion of the chain with it. Within this regime, active polymers may have substantially different signatures (Figs. 2F, 3F, S1). At lag times longer than τ_{Rse}, passive motion returns to diffusion, but this corresponds to the polymer center-of-mass motion [67]. For chromosomes, τ_{Rse} is typically very long and experimentally inaccessible. For this reason, we have not included this regime in Figs. 2F and 3F. The dynamic regimes of the active self-avoiding polymer are similar to that of the active Rouse chain (Supplementary Material, Fig. S1) [54, 55], since all the dynamic signatures originate from a competition between the monomer activity and the nearest neighbor bonds in the polymer potential.

Super-diffusion in active polymers

The leading order active contribution to MSD scales as quadratic in time $\sim (t/\tau)^2$, driving a super-diffusive regime [54, 55] (Supplementary Materials). Whereas, at the short time scales ($t \ll \tau_{\text{bond}}$), the thermal contribution is linear in lag time. This results in the MSD asymptotically approaching the diffusive (linear) regime near zero lag times irrespective of activity (Fig. 2F).

The activity-driven super diffusion in the MSD curves appears when the $\sim t^2$ active contribution exceeds the passive forces. The dominance of the active forces leads to a super-diffusive exponent when the lag time is comparable to the correlation time (Fig. 2F). For short correlation times ($\tau \approx \tau_{\text{bond}}$), the active polymer shows super-diffusion at the time scales of free-monomer dynamics (Fig. 2F).

For correlation times that are longer than the bond relaxation time ($\tau_{\text{bond}} < \tau < \tau_{\text{Rse}}$), the dynamics show a sub-diffusive regime at intermediate lag times: $\tau_{\text{bond}} < t < \tau$ (Fig. 2F). This sub-diffusion is a result of compensation of the persistent active drive by the polymer potential [54]. Interestingly, the entangled globule shows an extended sub-diffusive regime due to the suppression of dynamics in a crowded environment (Fig. 2F).

Active polymer dynamics restores to sub-diffusion at lag times longer than the correlation time (Fig. 2F). Within our model, at these long lag times, the active noise becomes indistinguishable in its time dependence from thermal noise. However, the motion is enhanced in amplitude due to the active noise contribution, reflected

in an increased apparent diffusivity.

Activity may enhance or suppress the apparent diffusivity

We compute an apparent diffusivity from the simulated MSD curves: $D_{\rm app} \equiv {\rm MSD}/t^{\alpha}$, where the exponent $\alpha \equiv \partial(\ln {\rm MSD})/\partial(\ln t)$. Note that the apparent diffusivity is a lag-time dependent coefficient that is equal to the diffusion constant when $\alpha = 1$. For lag times shorter than the bond relaxation time $\tau_{\rm bond}$, the apparent diffusivity for a passive polymer is set by the free-particle diffusion constant: $D_{\rm app} \approx k_B T/\gamma$ (Fig. 2F). While at lag times longer than the polymer relaxation time $t > \tau_{\rm Rse} > \tau$, the passive apparent diffusivity is again a constant: $D_{\rm app} \approx k_B T/(N\gamma)$, and is lower due to the center-of-mass motion [67].

The apparent diffusivity for active polymers shows enhancement over the corresponding passive behavior only for lag times longer than the correlation time (Fig. 2F). Interestingly, the active apparent diffusivity may also show suppression, such as in the entangled globule state. Competition between the active noise and the passive polymer potential underlies this suppression.

While super-diffusion is a unique characteristic of the active steady-state, investigating the dynamics at the appropriate lag time is essential to observe this. When lag times are longer than the active correlation time, the dynamics appear passive with a higher effective temperature (Fig. 2F). While lag times smaller than the correlation time may show suppressed dynamics akin to lower effective temperatures. Hence, observations of passive-like dynamic exponents do not rule out active forces, the apparent diffusivity and MSD exponents should be scrutinized at various lag times to investigate an active component.

Active dynamics bears another key signature: correlated motion of the monomers over long distances. Activity driven compact clusters exhibit correlated motion, reflected in a shallower decay of the two-point displacement correlation function for the active steady states (Fig. 2G).

Phase segregation of active and passive blocks of a confined self-avoiding polymer

To explore the effect of heterogeneity in activity along a polymer, we study a block copolymer with alternating active (A) and passive (P) blocks (Fig. 3A). The polymer has $N = 2000$ monomers and each alternating active and passive block of size $n = 200$ monomers. We use the same self-avoidance and confinement conditions ($\phi = 0.06$) as before (See Methods). In the passive-like regime ($T > \theta_a$), the A and P blocks mix due to entropy and the dynamics is equilibrium-like (Fig. 3F). The active steady states ($T < \theta_a$) tend to show phase segregation of A and P blocks. Spatial separation of two species with different dynamics underlies this segregation. Highly dynamic active monomers occupy a larger share of the confinement volume, relegating the passive monomers into a compact segregated state. Interestingly, the spatial organization of the segregated phases is governed by active correlation time (Fig. 3B, C, E).

Activity-driven phase separation between the active and passive blocks is observed only when the active force is large enough to release entanglements (Fig. 3B). Phase separation is measured via the coefficient μ, defined as the ratio of homotypic to heterotypic pairwise contacts between inter-block monomers. A pairwise contact is defined when the inter-monomer distance is less than 1.5σ (Methods). When $\mu > 1$ the active and passive blocks segregate, whereas $\mu < 1$ denotes the mixed state.

The entangled globule state shows an overall collapse of the entire polymer, where the active and passive blocks are not well segregated (Fig. 3B-E). The regime corresponding to boundary enrichment of the active blocks (high F and high τ), shows strong phase separation (Fig. 3B, C). In this regime, the passive blocks are highly compacted and reside at the center, while the active blocks spread over the boundary wall (Fig. 3E). Phase separation is also observed in the regime of low mean persistent path (high F and low τ). This state is characterized by compact passive domains and expanded, highly dynamic active blocks that are segregated without any radial preference, in a polar fashion (Fig. 3B-E). Increasing the thermal temperature releases entanglements for passive blocks and leads to a boundary enrichment of passive monomers (Fig. S6).

The dynamics of the active monomers in the block copolymer basically resemble the regimes explored in the active homopolymer case (Figs. 2F and 3F). Interestingly, the dynamics of the passive blocks show deviation from passive behavior (Fig. 3F). The bonded interactions with the active monomers make the passive blocks more dynamic.

Phase separation of passive block copolymers is typically modeled using the Flory-Huggins approach, where blocks are assigned self and mutual interactions. The active phase separation presented here is fundamentally different, as it is dynamically driven. Mutually repulsive active monomers segregate from the passive monomers creating regions of high and low dynamics. Although the structural ensembles of a Flory-Huggins polymer may appear similar to the active phase segregated system, the dynamics are more heterogeneous and span multiple regimes for the activity-driven structures.

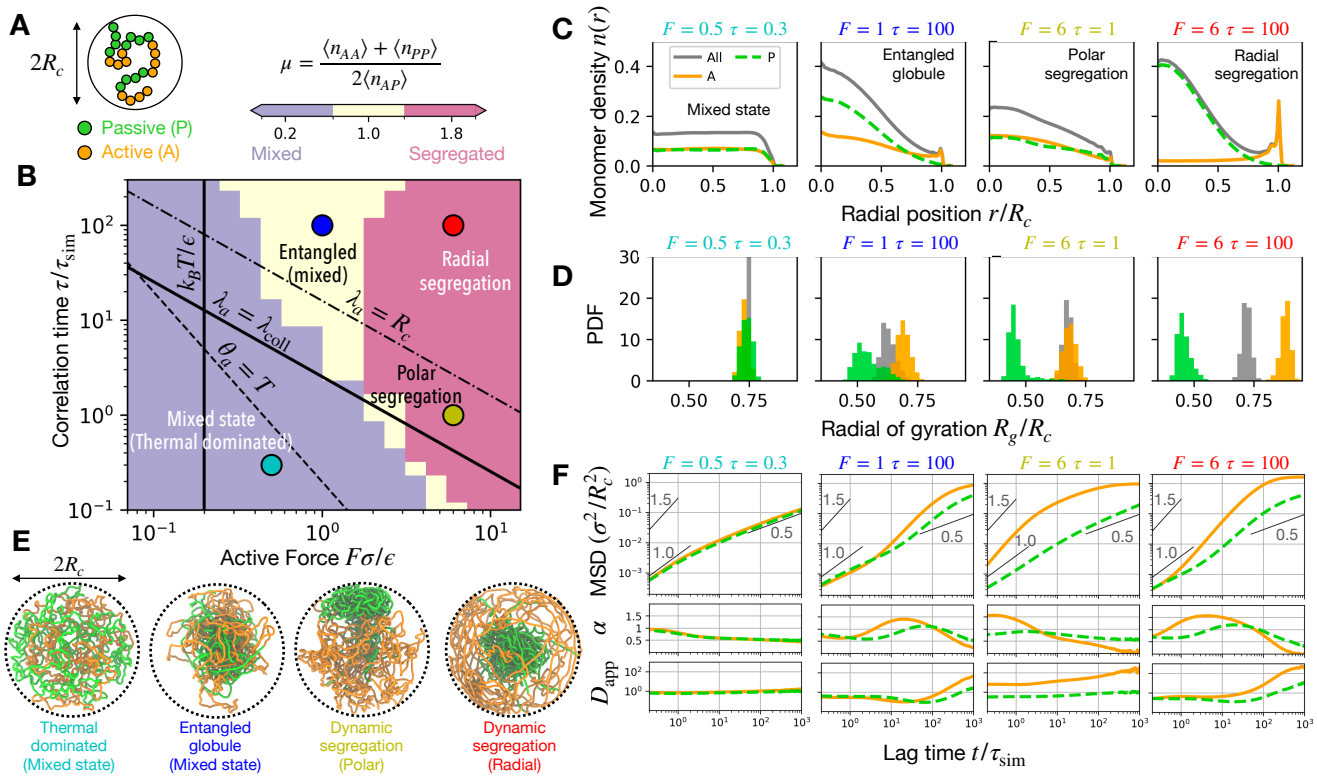

FIG. 3. **Phase separation of active and passive blocks of a confined self-avoiding polymer.** (A) Schematic showing the confined block copolymer with active (A) and passive (P) blocks with orange and green colors respectively. (B) Active regime diagram, where colors represent the phase separation coefficient μ, defined as the abundance of homotypic ($A-A$ and $P-P$) over heterotypic ($A-P$) contacts. When $\mu > 1$ (pink), there is segregation of the A and P blocks, while $\mu < 1$ (purple) signifies a mixed state. The active steady state generally shows a tendency to segregate the active and passive blocks due their altered dynamics. However, the entangled globule state is only marginally segregated due to topological constraints. Given the active force is strong enough to release entanglements, activity with $\lambda_a > R_c$ segregates the active and passive blocks radially. Otherwise, the passive blocks are segregated to a pole of the confinement. The four colored circles depict parameter sets for the four distinct regimes: thermal dominated ($F = 0.5$, $\tau = 0.3$, cyan), entangled globule ($F = 1$, $\tau = 100$, blue), polar segregation ($F = 6$, $\tau = 1$, yellow), and radial segregation ($F = 6$, $\tau = 100$, red). We used $k_BT = 0.2\epsilon$ for all simulations. (C) Radial profile of monomer density $n(r)$ for active (orange, solid lines), passive (green dashed lines), and all monomers (grey solid lines). (D) Radius of gyration of the active (orange), passive (green), and all monomers (grey). (E) Representative simulation snapshots with A and P monomers colored in orange and green respectively. (F) Mean-squared displacement (MSD), the dynamic exponent (α), and apparent diffusivity ($D_{\rm app}$) versus lag time, for active and passive monomers corresponding to the four regimes. The dynamics of the active monomers are the same as described before (Fig. 2C). The passive monomers deviate from a purely passive behavior due to their polymer connectivity with the highly dynamic active monomers.

Implications for chromosomes

Chromosomes are active matter, where motorized processes like transcription, loop extrusion, and chromatin remodeling are continually driving the structure and dynamics. Our understanding of chromosome folding and the underlying mechanics has consolidated thanks to the emulsification of experimental data like Hi-C contact maps [11–13] and polymer models [18–27]. However, the existing chromosome models are predominantly effective-equilibrium, lacking direct signatures of activity like superdiffusive chromatin loci [35, 38, 39].

We extend the presented active model to study chromosomes. The amplitude of the active noise is set by the typical stretching elasticity of chromatin: $F \approx 1-10$ pN [68, 69]. The active correlation time τ is a measure of the motor-residence time, which varies depending on the active process. While chromatin remodellers typically show fast, sub-second dynamics [43], persistent bursts of gene activity, corresponding to RNA polymerases moving processively, may last for many minutes [70]. Loop extruding enzymes typically extrude a 50 kb DNA loop in tens of seconds [45]. Note, extrusion activity of loops shorter than a monomer size ($\approx$ 50 kb) may be considered within this approach, whereas large loops spanning multiple monomers should be incorporated explicitly as large force dipoles. Hence, we argue that the physiological range for the correlation time is $\tau \approx 1-10^2$ seconds,

where the higher (lower) end of the spectrum is associated with transcription (chromatin remodeling and extrusion of short loops). Consequently, at experimentally realizable time scales (1-100 seconds), we expect chromatin regions housing highly transcribed genes to show super-diffusive signatures, whereas, loci containing loop extruders or chromatin remodellers are expected to show sub-diffusion with an enhanced apparent diffusivity.

The eukaryotic genome is typically confined within the nucleus with a volume fraction $\approx 1 - 10\%$ [65]. The hierarchical organization of the genome may introduce effective confinement with a similar volume fraction but at a smaller dimension. Such as the chromosome territories, which are about an order of magnitude smaller than the nuclear dimension, may effectively confine chromosomal loci, like genes or centromeres [10]. Hence there are multiple confinement lengthscales that may compete with the mean persistent path of an active chromosome locus.

Activity-driven collapse as a mechanism of chromosome compartmentalization

Compartmentalization is an important feature of chromosome folding in the interphase chromosomes of eukarya [11, 13, 16]. Compartments are globules formed by colocalization of sequentially distant genomic elements, reflected in the off-diagonal plaid-like patterns of the Hi-C maps. Hi-C-defined (sub)compartments are structural classes obtained via dimensionality reduction, e.g., Principal Component Analysis (PCA) of the pairwise genomic-interaction patterns [11, 13]. These compartments are correlated to the cellular gene expression profile and show tissue- or cell-type-specific variability [12, 71–73]. However, the mechanics governing the relationship between structurally annotated compartments and gene expression is not understood.

Polymer models typically invoke equilibrium phase separation (Flory-Huggins) as the driver of compartmentalization [18–27]. Chromosomes are represented as block copolymers where blocks may be defined via (sub)compartment annotations [18, 19] or epigenetics data like ChIP-Seq [23, 26, 74] and DamID [24]. Interblock interaction energies are then optimized, subject to polymeric constraints, to generate structural ensembles that reproduce experimental features like Hi-C maps. These structural ensembles correspond to a passive steady state exhibiting polymer subdiffusion, where heterogeneity in dynamics may only arise from suppression of diffusive motion by structural constraints like local compaction or confinement [33, 37].

It is clear from the discussed results (Figs. 2 and 3) that phase separation, akin to compartmentalization, may be recapitulated by the active model without any attractive interactions. As mentioned before, the distinguishing characteristic of activity is enhanced dynamics. Activity-driven chromatin compartments exhibit elevated apparent diffusivity with the possibility of a super-diffusive dynamic regime (Figs. 2C-E and 3F). These motor-driven compartments are stabilized by entanglement constraints. Hence, increased activity of enzymes like type-II DNA topoisomerase, releasing topological constraints, is expected to destabilize these compartments.

The motor-driven mechanism, however, does not rule out the possibility of short-range attractive interactions originating from the chemical nature (epigenetics) of the chromatin loci. Globules established via motor activity may act as a nucleation site for the three-dimensional spreading of epigenetic marks [75, 76]. This will lead to robust compartments that persist even when the motor activity ceases. Hence, we posit that the active (motor-driven) and passive (attractive interaction) mechanisms likely coexist, and propose that active and passive parameters be optimized simultaneously for a heterogeneous polymer such that the non-equilibrium steady state agrees with both the experimental structure (e.g, Hi-C maps [13]) and dynamics (distribution of MSDs [35]). However, such a detailed study is beyond the scope of the current work and is left for future research. Instead, we investigate the effect of adding activity to a handful of loci within a calibrated effective-equilibrium model, MiChroM [19, 48]. The objective here is to understand active perturbations to the effective-equilibrium structures of the passive model.

Passive compartments are expanded by active loci

The optimized MiChroM potential contains favorable inter-monomer interactions that may be divided into two categories: first, the phase separation term, and second, the ideal chromosome term that drives lengthwise compaction [19, 46]. The phase separation term drives the respective microphase separation of A and B-type monomers leading to segregated three-dimensional compartments. Lengthwise compaction represents polymer crumpling due to steady-state loop extrusion of SMC complexes and determines macroscopic chromosome shape [10, 46].

We simulate chromosome 10 of Human GM12878 cell at 50 kb resolution ($N = 2712$) using Eq. (1), where the passive forces ($-\nabla U$) originate from relaxation in the MiChroM potential. Additionally, we introduce seven active loci that model increased motor activity at those sites (Methods). We then studied how the structural ensembles change when the active loci correspond to three distinct regimes: passive ($F = 0$); active with short correlation time ($F = 5$, $\tau = 1$); and active with long correlation time ($F = 3$, $\tau = 30$) (Fig. 4). The passive case compares favorably with experimental data (Fig. S7),

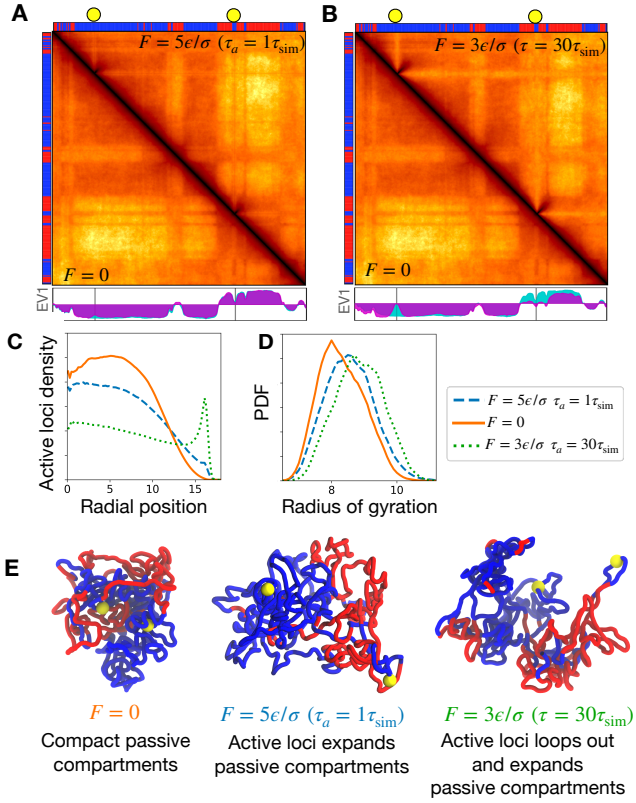

FIG. 4. **Active loci perturbs effective-equilibrium chromosome compartments.** (A) Simulated contact maps showing a 30 Mb segment (50 - 80 Mb) of the GM12878 chromosome 10. The lower triangle corresponds to the effective-equilibrium structure ($F = 0$), while the upper triangle corresponds to the active steady state with $F = 5$ and $\tau = 1$. The thermal temperature is $k_BT = 1.0\epsilon$. (B) Same as (A) with activity corresponding to a longer correlation time $F = 3$ and $\tau = 30$. The bars on the top and left of the contact maps show the A (red) and B (blue) type beads that drive A/B compartments via passive phase separation. The yellow circles denote the two active sites in the segment. The principal eigenvectors (EV1) are shown in the subpanel below, where the passive EV1 is colored in cyan and the active is colored in magenta. (C) Number density of active loci (including all the seven loci) plotted against radial position (σ units), showing a peripheral relocation of the loci for long correlation times. (D) Radius of gyration (σ units) of the 30 Mb segment plotted in the contact maps above, showing an expansion of passive compartments by activity. (E) Simulation snapshots of the 30 Mb segment containing two active loci shown as yellow spheres. The A-type regions are shown in red, while the B-type regions are shown in blue.

while the two active cases are in-silico experiments when motor activity is enhanced at the selected sites (Fig. 4).

The overall linear density of activity is kept low by design so that the effective equilibrium structures are largely preserved and we can study the local effect of activity on the passive structures. As expected, the contact maps only show variation near the active sites (Figs. 4A, B and S8). The most prominent effect was that the compartments carrying the active loci became expanded (Fig. 4D). This is a dynamics-driven phenomenon where activity agitates the local environment that counteracts the formation of passive compartments.

Activity with long correlation times drives chromosome loci territory edges and switch compartments

Active loci with long correlation times expand their respective compartments, additionally, they extend out of the compartment and tend to move towards the chromosome periphery (Figs. 4C, D, and S8). This leads to a light stripe in the simulated contact map, as the peripherally located active loci have limited interaction with the rest of the chromosome (Fig. 4B). Highly correlated activity may diminish the passive-compartment strength or altogether flip the compartment signature, as derived from PCA, at the active site (Fig. 4A, B).

Activity with a long correlation time captures persistent bursts of transcription that may last for minutes. Positioning of transcriptionally active segments to the periphery of chromosome territories is experimentally well-documented [15, 47, 77–80]. High transcriptional activity is correlated with long genes looping out of the chromosome territories [47]. The active model explains this as a direct consequence of the mechanics underlying the persistence of the transcription process in long, highly transcribed genes. The peripheral positioning of highly expressed genes leads to loss of contact with the rest of the chromosome, which has also been observed recently [81]. The active transcription mechanics can also drive switching of compartments, as has been observed during cellular differentiation [12, 72].

DISCUSSION

We studied a coarse-grained polymer model of chromosomes that, in addition to the uncorrelated thermal noise, experiences a temporally correlated active noise (Eqs. (1) and (2)). This active noise models the effect of microscopic motors exerting forces on the polymer (Fig. 1). We presented a simplified characterization of the steady state of the active polymer using two parameters: the force F depicting the active noise amplitude and the correlation time τ controlling the temporal persistence of the active noise (Figs. 2A and 3B). The model exhibits diverse structural and dynamic properties. Active-polymer dynamics span sub-diffusion, effective diffusion, and super-diffusion, where the correlated active kicks underlie the super-diffusive regime (Figs. 2F and 3F). Importantly, non-equilibrium activity can result not only in enhanced monomer dynamics (e.g., super-diffusion) but also in structure formation that arises from

stochastic active forces. Contrasting features like polymer swelling/collapse and radial phase segregation with higher monomer density towards the center/periphery, are some of the actively controlled structural aspects (Figs. 2B-D and 3C-E). The active steady-state structures may look similar to that of a passive system with attractive or repulsive interactions between monomers, however, the underlying mechanisms are completely different (Figs. 2D and 3E) the dynamics is essential to distinguish between active and passive mechanisms.

We propose motor-driven collapse as a mechanism of chromosome compartmentalization. These compartments are entanglement driven, such that they can be destabilized via enzymes like type-II DNA topoisomerases that release entanglements. Upon entanglement release, the segments with correlated activity, such as highly transcribed genes, move toward the periphery of chromosomes. This suggests that the mechanics of transcription is contributing to the relocation of the highly transcribed genes to chromosome territory edges. We also found that the compartments established by passive forces like phase separation are destabilized by activity due to the enhanced local dynamics (Fig. 4). Recent modeling has proposed that activity correlated along the polymer chain may drive compartmentalization [57]. Our model shows that compartment-like compaction can also arise from an interplay of entanglements and temporally correlated activity.

Cell-type-specific variations in the genome architecture are reflected in the compartment structure [12, 71–73]. These observations posit a conundrum: do compartments drive gene expression or vice-versa? While it is conceivable that the distinct chemical microenvironments within compartments help recruit transcription machinery thus aiding gene expression, our results suggest there is mechanical feedback wherein a highly transcribed locus may alter the compartment structure surrounding the locus. Investigating the causality between compartments and gene expression is key to deciphering the genome structure-to-function relationship.

Chromatin loci typically show sub-diffusion, which may be either passive or active in nature [28–31, 82, 83]. Effective equilibrium models are consistent with sub-diffusive dynamics [33, 37, 84, 85]. Interestingly, experiments have confirmed the presence of a wide distribution of dynamic exponents, including super-diffusion [35, 38, 39], which must be active in nature. There are also observations of multiple sub-populations with distinct apparent diffusion constants [32–36]. The active model proposes that heterogeneous loci dynamics arise from heterogeneity in motor activity (Figs. 2F and 3F).

Existing non-equilibrium models of flexible biopolymers have previously discussed some of the results we described here. By explicitly modeling motors that may bind the polymer and apply forces, the possibility of a super-diffusive regime in the intermediate time scales has been discussed [86]. Using locus-specific effective temperatures has been yet another approach to recapitulate nonequilibrium aspects [87, 88], however, the possibility of super-diffusion is not within the scope of such approaches. Phenomenological modeling of active forces with hydrodynamics has been useful in understanding coherent motions in the genome [53, 89]. There are also models that use an approach similar to the one used here and discuss the emergence of super-diffusivity [54, 55, 64] and collapse [90]. The active model presented here puts into perspective the observations of these models and proposes a novel, intuitive characterization of the active steady state, as represented in the phase diagrams (Figs. 2A and 3B). This model opens the avenue to incorporate motor activity in coarse-grained chromosomes using a simple two-parameter description, that avoids explicit modeling of motors. We hope this work will lead to many new non-equilibrium models of chromosomes, and aid in the design of future experiments investigating the signatures of motor activity in chromosomes.

METHODS

Brownian Dynamics Simulations. We simulate the equation of motion for each particle (Eq. (1)) using a custom integrator within the OpenMiChroM simulation package [48]. The integrator computes the active noise $f(t)$ at each time step by integrating the following equation for each particle: $\tau \partial f/\partial t = -f(t) + \sqrt{2\gamma\theta_a}\eta(t)$, where η is a delta-correlated stationary Gaussian process with zero mean, and $\gamma = 1.0\epsilon\tau_{\text{sim}}/\sigma^2$ is the drag coefficient.

Polymer potential. The polymer potential constitutes of two terms: bonding between nearest neighbors and a short-range inter-monomer repulsion to simulate self-avoidance. The nearest neighbors along the polymer chain are bonded using a linear spring: $U_{nn} = (k/2)(r - d)^2$, where k is the spring constant and d is the unperturbed bond length. We use $k = 30\epsilon/\sigma^2$ unless otherwise mentioned. Here ϵ is the reduced unit of energy. For Rouse chains we used $d = 0$ while for all else we set $d = 1\sigma$.

Self avoidance is modeled using a pairwise soft-core repulsive potential of the form: $U_{sa}(r) = (E_0/2)(1 + \tanh(1 - k_{sa}(r - d_{sa})))$, where $k_{sa} = 20\epsilon/\sigma^2$ encodes the steepness of the repulsion, $d_{sa} = 1\sigma$ is typical distance below which repulsion kicks in, and $E_0 = 5\epsilon$ is the maximum repulsive energy.

Finally, there is the spherical-confinement potential. We use a flat-bottom harmonic or half-harmonic restraint for the confinement: $U_{conf} = (k_{conf}/2)(r - R_c)^2\Theta(r - R_c)$, where $\Theta(r - R_c)$ is the Heavy-side theta function that is zero when $r < R_c$ and one when $r \geq R_c$. We use $k_{conf} = 30\epsilon/\sigma^2$ throughout this work.

Chromosome potential. For the chromosome potential We utilize the optimized MiChroM parameters [19, 48] to simulate the passive forces within our Brownian dynamics scheme (Eq. 1). We chose chromosome 10 of Human GM12878 cell line, which has $N = 2711$ beads with each bead representing 50 kb DNA. The active loci were selected to be at the monomer indices: 99,376,740,1100,1432,1860,2340. We then studied the effect on the passive structure as the activity was turned on for the active loci.

Steady-state trajectories. Starting from random configurations, the polymer is equilibrated at temperature T. We used $k_BT = 0.2\epsilon$ for simulations unless otherwise mentioned. Then, activity with a fixed F and τ is turned on for every monomer, and simulations are run for 10^6 time steps with integration step $dt = 10^{-3}\tau_{\text{sim}}$ to establish the active steady state. We also used the analytical calculations of the Rouse polymer as a verification step for our simulations (Supplementary Materials). Steady-state simulation for each parameter set was run for $10^4\tau_{\text{sim}}$, saving the particle coordinates every $0.1\tau_{\text{sim}}$. We simulated multiple replicas for each parameter for statistical analyses. All reported quantities, like the radius of gyration, monomer density, and MSD, were computed from the steady-state trajectories. These quantities are also averaged over the ensemble.

Monomer density. The monomer density $n(r)$ is computed by counting the number of monomers in concentric shells, such that: $\int_0^{R_c} 4\pi r^2 n(r)dr = N$, where N is the total number of monomers.

Radial distribution function. The radial distribution function is computed from the standard definition: $g(r) = dn_r\sigma^3/(4\pi r^2 dr\phi)$, where dn_r is the number of monomers within distance r and $r + dr$ from the center.

Displacement correlation between particles. The spatial correlation of displacements between particles was computed using the formula: $C_x(\Delta r, \Delta t) = \left\langle \frac{1}{n}\sum_n \frac{\vec{d}_i(r,\Delta t)\cdot\vec{d}_j(r+\Delta r,\Delta t)}{\sqrt{d_i^2(r,\Delta t)\ d_j^2(r+\Delta r,\Delta t)}} \right\rangle$, where $d_i(r, \Delta t)$ is the displacement of the i-th particle located at r over a lag time Δt and d_j is the corresponding displacement of the j-th particle that is located a distance Δr away from the i-the particle. The displacement correlation is summed over for all the n particles that lie within a sphere of radius Δr, and the angular bracket denotes averaging over the trajectories.

Phase-separation coefficient. The phase-separation coefficient μ is defined as: $\mu \equiv (\langle n_{AA}\rangle + \langle n_{PP}\rangle)/\langle 2n_{AP}\rangle$. Here, n_{AA} is the number of pairwise contacts between A blocks (homotypic contacts), and n_{PP} (homotypic) and n_{AP} (heterotypic) are similarly defined. Two monomers are defined to be in contact when the distance between them is less than 1.5σ. Contacts between monomers of the same block are ignored to enhance the inter-block phase separation signal.

Active regime diagrams. Steady-state trajectories were generated for a logarithmically spaced grid with F varying between $0 - 15\epsilon/\sigma$ and τ varying between $0.1 - 300\tau_{\text{sim}}$. The observables like the radius of gyration was computed for the above-mentioned grid and then interpolated into a finer grid to plot the active regime diagrams (Figs. 2A, 3B).

Contact maps. The contact maps were generated using the procedure described in Refs. [19, 48]. The pairwise distance between monomers r_{ij} is converted to probability using the previously optimized sigmoid function $f_{\text{contact}}(r_{ij}) = 0.5 * (1 + \tanh(3.22 * (1.78 - r_{ij})))$ [19, 48].

A tutorial on how to run the active simulations can be found at https://github.com/s-brahmachari/ActiveOpenMiChroM/tree/main/Tutorials/Active_Chromosome_Dynamics. The simulation snapshots were generated using the Visual Molecular Dynamics (VMD) software http://www.ks.uiuc.edu/Research/vmd/.

ACKNOWLEDGMENTS

This work was supported by the Center for Theoretical Biological Physics (CTBP) sponsored by the National Science Foundation (NSF Grants PHY-2019745, PHY-2210291 and DMR-2224030) and by the Welch Foundation (Grant C-1792). We are grateful for the computational resources provided by Advanced Micro Devices (AMD). JNO is a Cancer Prevention and Research Institute of Texas (CPRIT) Scholar in Cancer Research. SB acknowledges the Robert A. Welch Postdoctoral Fellow program. We would like to thank Peter Wolynes, Vinicius G. Contessoto, Antonio Oliveira Jr., and other members of CTBP for helpful discussions.

* sb95@rice.edu

[1] D. Mizuno, C. Tardin, C. F. Schmidt, and F. C. MacKintosh, Nonequilibrium mechanics of active cytoskeletal networks, Science **315**, 370 (2007).

[2] P. M. Bendix, G. H. Koenderink, D. Cuvelier, Z. Dogic, B. N. Koeleman, W. M. Brieher, C. M. Field, L. Mahadevan, and D. A. Weitz, A quantitative analysis of contractility in active cytoskeletal protein networks, Biophysical Journal **94**, 3126 (2008).

[3] S. Wang and P. G. Wolynes, Active contractility in actomyosin networks, Proceedings of the National Academy of Sciences of the United States of America **109**, 6446 (2012).

[4] S. Wang and P. G. Wolynes, On the spontaneous collective motion of active matter, Proceedings of the National Academy of Sciences of the United States of America **108**, 15184 (2011).

[5] E. Tjhung, D. Marenduzzo, and M. E. Cates, Spontaneous symmetry breaking in active droplets provides a generic route to motility, Proceedings of the National

Academy of Sciences of the United States of America **109**, 12381 (2012).

[6] L. Blanchoin, R. Boujemaa-Paterski, C. Sykes, and J. Plastino, Actin dynamics, architecture, and mechanics in cell motility, Physiological Reviews **94**, 235 (2014).

[7] V. Hakim and P. Silberzan, Collective cell migration: a physics perspective, Reports on Progress in Physics **80**, 076601 (2017).

[8] T. Cremer and C. Cremer, Chromosome territories, nuclear architecture and gene regulation in mammalian cells, Nature Reviews Genetics 2001 2:4 **2**, 292 (2001).

[9] W. A. Bickmore, The spatial organization of the human genome 10.1146/annurev-genom-091212-153515 (2013).

[10] C. Hoencamp, O. Dudchenko, A. M. Elbatsh, S. Brahmachari, J. A. Raaijmakers, T. van Schaik, Ángela Sedeño Cacciatore, V. G. Contessoto, R. G. van Heesbeen, B. van den Broek, A. N. Mhaskar, H. Teunissen, B. G. S. Hilaire, D. Weisz, A. D. Omer, M. Pham, Z. Colaric, Z. Yang, S. S. Rao, N. Mitra, C. Lui, W. Yao, R. Khan, L. L. Moroz, A. Kohn, J. S. Leger, A. Mena, K. Holcroft, M. C. Gambetta, F. Lim, E. Farley, N. Stein, A. Haddad, D. Chauss, A. S. Mutlu, M. C. Wang, N. D. Young, E. Hildebrandt, H. H. Cheng, C. J. Knight, T. L. Burnham, K. A. Hovel, A. J. Beel, P. J. Mattei, R. D. Kornberg, W. C. Warren, G. Cary, J. L. Gómez-Skarmeta, V. Hinman, K. Lindblad-Toh, F. D. Palma, K. Maeshima, A. S. Multani, S. Pathak, L. Nel-Themaat, R. R. Behringer, P. Kaur, R. H. Medema, B. van Steensel, E. de Wit, J. N. Onuchic, M. D. Pierro, E. L. Aiden, and B. D. Rowland, 3d genomics across the tree of life reveals condensin ii as a determinant of architecture type, Science (New York, N.Y.) **372**, 10.1126/SCIENCE.ABE2218 (2021).

[11] E. Lieberman-aiden, N. L. V. Berkum, L. Williams, M. Imakaev, T. Ragoczy, A. Telling, I. Amit, B. R. Lajoie, P. J. Sabo, M. O. Dorschner, R. Sandstrom, B. Bernstein, M. A. Bender, M. Groudine, A. Gnirke, J. Stamatoyannopoulos, and L. A. Mirny, Comprehensive mapping of long-range interactions reveals folding principles of the human genome, Science **33292**, 289 (2009).

[12] J. R. Dixon, I. Jung, S. Selvaraj, Y. Shen, J. E. Antosiewicz-Bourget, A. Y. Lee, Z. Ye, A. Kim, N. Rajagopal, W. Xie, Y. Diao, J. Liang, H. Zhao, V. V. Lobanenkov, J. R. Ecker, J. A. Thomson, and B. Ren, Chromatin architecture reorganization during stem cell differentiation, Nature **518**, 331 (2015).

[13] S. S. P. Rao, M. H. Huntley, N. C. Durand, E. K. Stamenova, I. D. Bochkov, J. T. Robinson, A. L. Sanborn, I. Machol, A. D. Omer, E. S. Lander, and E. Lieberman-Aiden, Article a 3d map of the human genome at kilobase resolution reveals principles of chromatin looping, Cell **159**, 1665 (2014).

[14] A. N. Boettiger, B. Bintu, J. R. Moffitt, S. Wang, B. J. Beliveau, G. Fudenberg, M. Imakaev, L. A. Mirny, C. T. Wu, and X. Zhuang, Super-resolution imaging reveals distinct chromatin folding for different epigenetic states, Nature 2016 529:7586 **529**, 418 (2016).

[15] B. Bintu, L. J. Mateo, J.-H. Su, N. A. Sinnott-Armstrong, M. Parker, S. Kinrot, K. Yamaya, A. N. Boettiger, and X. Zhuang, Super-resolution chromatin tracing reveals domains and cooperative interactions in single cells, Science **362**, eaau1783 (2018).

[16] E. M. Hildebrand and J. Dekker, Mechanisms and functions of chromosome compartmentalization, Trends in biochemical sciences **45**, 385 (2020).

[17] J. H. Su, P. Zheng, S. S. Kinrot, B. Bintu, and X. Zhuang, Genome-scale imaging of the 3d organization and transcriptional activity of chromatin, Cell **182**, 1641 (2020).

[18] M. Falk, Y. Feodorova, N. Naumova, M. Imakaev, B. R. Lajoie, H. Leonhardt, B. Joffe, J. Dekker, G. Fudenberg, I. Solovei, and L. A. Mirny, Heterochromatin drives compartmentalization of inverted and conventional nuclei, Nature 2019 570:7761 **570**, 395 (2019).

[19] M. D. Pierro, B. Zhang, E. L. Aiden, P. G. Wolynes, and J. N. Onuchic, Transferable model for chromosome architecture, Proceedings of the National Academy of Sciences of the United States of America **113**, 12168 (2016).

[20] Y. Qi, A. Reyes, S. E. Johnstone, M. J. Aryee, B. E. Bernstein, and B. Zhang, Data-driven polymer model for mechanistic exploration of diploid genome organization, Biophysical Journal **119**, 1905 (2020).

[21] A. Esposito, S. Bianco, A. M. Chiariello, A. Abraham, L. Fiorillo, M. Conte, R. Campanile, and M. Nicodemi, Polymer physics reveals a combinatorial code linking 3d chromatin architecture to 1d chromatin states, Cell Reports **38**, 10.1016/J.CELREP.2022.110601 (2022).

[22] H. Wong, H. Marie-Nelly, S. Herbert, P. Carrivain, H. Blanc, R. Koszul, E. Fabre, and C. Zimmer, A predictive computational model of the dynamic 3d interphase yeast nucleus, Current Biology **22**, 1881 (2012).

[23] D. Jost, P. Carrivain, G. Cavalli, and C. Vaillant, Modeling epigenome folding: Formation and dynamics of topologically associated chromatin domains, Nucleic Acids Research **42**, 9553 (2014).

[24] M. Chiang, D. Michieletto, C. A. Brackley, N. Rattanavirotkul, H. Mohammed, D. Marenduzzo, and T. Chandra, Polymer modeling predicts chromosome reorganization in senescence, Cell Reports **28**, 3212 (2019).

[25] G. Shi and D. Thirumalai, From hi-c contact map to three-dimensional organization of interphase human chromosomes, Physical Review X **11**, 10.1103/PhysRevX.11.011051 (2021).

[26] Q. MacPherson, B. Beltran, and A. J. Spakowitz, Bottom–up modeling of chromatin segregation due to epigenetic modifications, Proceedings of the National Academy of Sciences of the United States of America **115**, 12739 (2018).

[27] S. Fujishiro and M. Sasai, Generation of dynamic three-dimensional genome structure through phase separation of chromatin, Proceedings of the National Academy of Sciences of the United States of America **119**, e2109838119 (2022).

[28] I. Bronstein, Y. Israel, E. Kepten, S. Mai, Y. Shav-Tal, E. Barkai, and Y. Garini, Transient anomalous diffusion of telomeres in the nucleus of mammalian cells 10.1103/PhysRevLett.103.018102 (2009).

[29] H. Hajjoul, J. Mathon, H. Ranchon, I. Goiffon, J. Mozziconacci, B. Albert, P. Carrivain, J. M. Victor, O. Gadal, K. Bystricky, and A. Bancaud, High-throughput chromatin motion tracking in living yeast reveals the flexibility of the fiber throughout the genome, Genome Research **23**, 1829 (2013).

[30] A. Zidovska, D. A. Weitz, and T. J. Mitchison, Micron-scale coherence in interphase chromatin dynamics., Proceedings of the National Academy of Sciences of the United States of America **110**, 15555 (2013).

[31] S. C. Weber, A. J. Spakowitz, and J. A. Theriot, Nonthermal atp-dependent fluctuations contribute to the in vivo motion of chromosomal loci, Proceedings of the National Academy of Sciences of the United States of America **109**, 7338 (2012).

[32] B. Gu, T. Swigut, A. Spencley, M. R. Bauer, M. Chung, T. Meyer, and J. Wysocka, Transcription-coupled changes in nuclear mobility of mammalian cis-regulatory elements, Science **359**, 1050 (2018).

[33] S. S. Ashwin, T. Nozaki, K. Maeshima, and M. Sasai, Organization of fast and slow chromatin revealed by single-nucleosome dynamics, Proceedings of the National Academy of Sciences of the United States of America **116**, 19939 (2019).

[34] H. Ma, L.-C. Tu, Y.-C. Chung, A. Naseri, D. Grunwald, S. Zhang, and T. Pederson, Cell cycle-and genomic distance-dependent dynamics of a discrete chromosomal region 10.1083/jcb.201807162 (2019).

[35] H. A. Shaban, R. Barth, L. Recoules, and K. Bystricky, Hi-d: Nanoscale mapping of nuclear dynamics in single living cells, Genome Biology **21**, 1 (2020).

[36] J. Lerner, P. A. Gomez-Garcia, R. L. McCarthy, Z. Liu, M. Lakadamyali, and K. S. Zaret, Two-parameter mobility assessments discriminate diverse regulatory factor behaviors in chromatin, Molecular Cell **79**, 677 (2020).

[37] H. Salari, M. D. Stefano, and D. Jost, Spatial organization of chromosomes leads to heterogeneous chromatin motion and drives the liquid- or gel-like dynamical behavior of chromatin, Genome research **32**, 28 (2022).

[38] A. Javer, N. J. Kuwada, Z. Long, V. G. Benza, K. D. Dorfman, P. A. Wiggins, P. Cicuta, and M. C. Lagomarsino, Persistent super-diffusive motion of escherichia coli chromosomal loci 10.1038/ncomms4854 (2014).

[39] I. Eshghi, J. A. Eaton, and A. Zidovska, Interphase chromatin undergoes a local sol-gel transition upon cell differentiation 10.1103/PhysRevLett.126.228101 (2021).

[40] J. Gelles and R. Landick, Rna polymerase as a molecular motor, Cell **93**, 13 (1998).

[41] J. Ma, L. Bai, and M. D. Wang, Transcription under torsion, Science (New York, N.Y.) **340**, 1580 (2013).

[42] F. R. Neumann, V. Dion, L. R. Gehlen, M. Tsai-Pflugfelder, R. Schmid, A. Taddei, and S. M. Gasser, Targeted ino80 enhances subnuclear chromatin movement and ectopic homologous recombination, Genes and Development **26**, 369 (2012).

[43] J. M. Kim, P. Visanpattanasin, V. Jou, S. Liu, X. Tang, Q. Zheng, K. Y. Li, J. Snedeker, L. D. Lavis, T. Lionnet, and C. Wu, Single-molecule imaging of chromatin remodelers reveals role of atpase in promoting fast kinetics of target search and dissociation from chromatin, eLife **10**, 10.7554/ELIFE.69387 (2021).

[44] M. Ganji, I. A. Shaltiel, S. Bisht, E. Kim, A. Kalichava, C. H. Haering, and C. Dekker, Real-time imaging of dna loop extrusion by condensin, Science **360**, 102 (2018).

[45] S. Golfier, T. Quail, H. Kimura, and J. Brugués, Cohesin and condensin extrude dna loops in a cell-cycle dependent manner, eLife **9**, 1 (2020).

[46] S. Brahmachari, V. G. Contessoto, M. D. Pierro, and J. D. N. Onuchic, Shaping the genome via lengthwise compaction, phase separation, and lamina adhesion, Nucleic Acids Research **50**, 4258 (2022).

[47] S. Leidescher, J. Ribisel, S. Ullrich, Y. Feodorova, E. Hildebrand, A. Galitsyna, S. Bultmann, S. Link, K. Thanisch, C. Mulholland, J. Dekker, H. Leonhardt, L. Mirny, and I. Solovei, Spatial organization of transcribed eukaryotic genes, Nature Cell Biology 2022 24:3 **24**, 327 (2022).

[48] A. B. O. Junior, V. G. Contessoto, M. F. Mello, and J. N. Onuchic, A scalable computational approach for simulating complexes of multiple chromosomes, Journal of molecular biology **433**, 10.1016/J.JMB.2020.10.034 (2021).

[49] A. W. Lau, B. D. Hoffman, A. Davies, J. C. Crocker, and T. C. Lubensky, Microrheology, stress fluctuations, and active behavior of living cells, Physical Review Letters **91**, 198101 (2003).

[50] Y. Hatwalne, S. Ramaswamy, M. Rao, and R. A. Simha, Rheology of active-particle suspensions, The American Physical Society **92**, 118101 (2004).

[51] F. C. Mackintosh and A. J. Levine, Nonequilibrium mechanics and dynamics of motor-activated gels 10.1103/PhysRevLett.100.018104 (2008).

[52] M. C. Marchetti, J. F. Joanny, S. Ramaswamy, T. B. Liverpool, J. Prost, M. Rao, and R. A. Simha, Hydrodynamics of soft active matter 10.1103/RevModPhys.85.1143 (2013).

[53] R. Bruinsma, A. Y. Grosberg, Y. Rabin, and A. Zidovska, Chromatin hydrodynamics, Biophysical Journal **106**, 1871 (2014).

[54] D. Osmanović and Y. Rabin, Dynamics of active rouse chains, Soft Matter **13**, 963 (2017).

[55] A. Ghosh and A. J. Spakowitz, Statistical behavior of nonequilibrium and living biological systems subjected to active and thermal fluctuations, Physical Review E **105**, 14415 (2022).

[56] A. Caspi, R. Granek, and M. Elbaum, Enhanced diffusion in active intracellular transport, Physical Review Letters **85**, 5655 (2000).

[57] A. Goychuk, D. Kannan, A. K. Chakraborty, and M. Kardar, Polymer folding through active processes recreates features of genome organization, bioRxiv , 2022.12.24.521789 (2022).

[58] T. Markovich, E. Tjhung, and M. E. Cates, Chiral active matter: microscopic 'torque dipoles' have more than one hydrodynamic description, (2019).

[59] N. Fakhri, A. D. Wessel, C. Willms, M. Pasquali, D. R. Klopfenstein, F. C. MacKintosh, and C. F. Schmidt, High-resolution mapping of intracellular fluctuations using carbon nanotubes, Science **344**, 1031 (2014).

[60] M. Guo, A. J. Ehrlicher, M. H. Jensen, M. Renz, J. R. Moore, R. D. Goldman, J. Lippincott-Schwartz, F. C. Mackintosh, and D. A. Weitz, Probing the stochastic, motor-driven properties of the cytoplasm using force spectrum microscopy, Cell **158**, 822 (2014).

[61] D. Martin, J. O'Byrne, M. E. Cates, Étienne Fodor, C. Nardini, J. Tailleur, and F. V. Wijland, Statistical mechanics of active ornstein-uhlenbeck particles, Physical Review E **103**, 10.1103/PhysRevE.103.032607 (2021).

[62] C. Maggi, M. Paoluzzi, N. Pellicciotta, A. Lepore, L. Angelani, and R. D. Leonardo, Generalized energy equipartition in harmonic oscillators driven by active baths 10.1103/PhysRevLett.113.238303 (2014).

[63] M. E. Cates and J. Tailleur, Motility-induced phase separation, Annual Review of Condensed Matter Physics **6**, 219 (2015).

[64] A. Ghosh and A. J. Spakowitz, Active and thermal fluctuations in multi-scale polymer structure and dynamics,

Soft Matter **18**, 6629 (2022).

[65] S. Brahmachari and J. F. Marko, Chromosome disentanglement driven via optimal compaction of loop-extruded brush structures, Proceedings of the National Academy of Sciences , 201906355 (2019).

[66] J. Stenhammar, D. Marenduzzo, R. J. Allen, and M. E. Cates, Phase behaviour of active brownian particles: the role of dimensionality, Soft Matter **10**, 1489 (2014).

[67] M. Doi and S. F. Edwards, *The Theory of Polymer Dynamics* (Clarendon Press, 1988).

[68] Y. Cui and C. Bustamante, Pulling a single chromatin fiber reveals the forces that maintain its higher-order structure, Proceedings of the National Academy of Sciences of the United States of America **97**, 127 (2000).

[69] H. Yin, M. D. Wang, K. Svoboda, R. Landick, S. M. Block, and J. Gelles, Transcription against an applied force, Science **270**, 1653 (1995).

[70] B. T. Donovan, A. Huynh, D. A. Ball, H. P. Patel, M. G. Poirier, D. R. Larson, M. L. Ferguson, and T. L. Lenstra, Live-cell imaging reveals the interplay between transcription factors, nucleosomes, and bursting, The EMBO Journal **38**, 10.15252/embj.2018100809 (2019).

[71] D. Kurotaki, K. Kikuchi, K. Cui, W. Kawase, K. Saeki, J. Fukumoto, A. Nishiyama, K. Nagamune, K. Zhao, K. Ozato, P. P. Rocha, and T. Tamura, Chromatin structure undergoes global and local reorganization during murine dendritic cell development and activation, Proceedings of the National Academy of Sciences of the United States of America **119**, e2207009119 (2022).

[72] R. Vilarrasa-Blasi, P. Soler-Vila, N. Verdaguer-Dot, N. Russiñol, M. D. Stefano, V. Chapaprieta, G. Clot, I. Farabella, P. Cuscó, M. Kulis, X. Agirre, F. Prosper, R. Beekman, S. Beà, D. Colomer, H. G. Stunnenberg, I. Gut, E. Campo, M. A. Marti-Renom, José, and I. Martin-Subero, Dynamics of genome architecture and chromatin function during human b cell differentiation and neoplastic transformation 10.1038/s41467-020-20849-y.

[73] B. Bonev, N. M. Cohen, Q. Szabo, L. Fritsch, G. L. Papadopoulos, Y. Lubling, X. Xu, X. Lv, J. P. Hugnot, A. Tanay, and G. Cavalli, Multiscale 3d genome rewiring during mouse neural development, Cell **171**, 557 (2017).

[74] M. D. Pierro, R. R. Cheng, E. L. Aiden, P. G. Wolynes, and J. N. Onuchic, De novo prediction of human chromosome structures: Epigenetic marking patterns encode genome architecture, Proceedings of the National Academy of Sciences **114**, 12126 (2017).

[75] D. Michieletto, M. Chiang, D. Colì, A. Papantonis, E. Orlandini, P. R. Cook, and D. Marenduzzo, Shaping epigenetic memory via genomic bookmarking, Nucleic Acids Research **46**, 83 (2018).

[76] J. A. Owen, D. Osmanovi´cosmanovi´c, and L. A. Mirny, Design principles of 3d epigenetic memory systems, bioRxiv , 2022.09.24.509332 (2022).

[77] N. L. Mahy, P. E. Perry, and W. A. Bickmore, Gene density and transcription influence the localization of chromatin outside of chromosome territories detectable by fish, The Journal of Cell Biology **159**, 753 (2002).

[78] T. Nagano, Y. Lubling, T. J. Stevens, S. Schoenfelder, E. Yaffe, W. Dean, E. D. Laue, A. Tanay, and P. Fraser, Single cell hi-c reveals cell-to-cell variability in chromosome structure, Nature **502**, 59 (2013).

[79] S. Chambeyron and W. A. Bickmore, Chromatin decondensation and nuclear reorganization of the hoxb locus upon induction of transcription, Genes development **18**, 1119 (2004).

[80] R. R. Williams, S. Broad, D. Sheer, and J. Ragoussis, Subchromosomal positioning of the epidermal differentiation complex (edc) in keratinocyte and lymphoblast interphase nuclei, Experimental Cell Research **272**, 163 (2002).

[81] W. Winick-Ng, A. Kukalev, I. Harabula, L. Zea-Redondo, D. Szabó, M. Meijer, L. Serebreni, Y. Zhang, S. Bianco, A. M. Chiariello, I. Irastorza-Azcarate, C. J. Thieme, T. M. Sparks, S. Carvalho, L. Fiorillo, F. Musella, E. Irani, E. T. Triglia, A. A. Kolodziejczyk, A. Abentung, G. Apostolova, E. J. Paul, V. Franke, R. Kempfer, A. Akalin, S. A. Teichmann, G. Dechant, M. A. Ungless, M. Nicodemi, L. Welch, G. Castelo-Branco, and A. Pombo, Cell-type specialization is encoded by specific chromatin topologies, Nature 2021 599:7886 **599**, 684 (2021).

[82] F. C. MacKintosh, Active diffusion: The erratic dance of chromosomal loci, Proceedings of the National Academy of Sciences of the United States of America **109**, 7138 (2012).

[83] K. Smith, B. Griffin, H. Byrd, F. C. Mackintosh, and M. L. Kilfoil, Nonthermal fluctuations of the mitotic spindle, Soft Matter **11**, 4396 (2015).

[84] A. Rosa and R. Everaers, Structure and dynamics of interphase chromosomes, PLOS Computational Biology **4**, e1000153 (2008).

[85] M. D. Pierro, D. A. Potoyan, P. G. Wolynes, and J. N. Onuchic, Anomalous diffusion, spatial coherence, and viscoelasticity from the energy landscape of human chromosomes, Proceedings of the National Academy of Sciences **115**, 7753 (2018).

[86] M. Foglino, E. Locatelli, C. A. Brackley, D. Michieletto, C. N. Likos, and D. Marenduzzo, Non-equilibrium effects of molecular motors on polymers, Soft Matter **15**, 5995 (2019).

[87] A. Agrawal, N. Ganai, S. Sengupta, and G. I. Menon, Nonequilibrium biophysical processes influence the large-scale architecture of the cell nucleus, Biophysical Journal **118**, 2229 (2020).

[88] P. Bera, A. Wasim, and J. Mondal, Hi-c embedded polymer model of escherichia coli reveals the origin of heterogeneous subdiffusion in chromosomal loci, Physical Review E **105**, 064402 (2022).

[89] D. Saintillan, M. J. Shelley, and A. Zidovska, Extensile motor activity drives coherent motions in a model of interphase chromatin., Proceedings of the National Academy of Sciences of the United States of America **115**, 11442 (2018).

[90] Z. Jiang, Y. Qi, K. Kamat, and B. Zhang, Phase separation and correlated motions in motorized genome, Journal of Physical Chemistry B **126**, 5619 (2022).